ACS Catalysis

Research Article

pubs.acs.org/acscatalysis

Operando Time-Resolved X-ray Absorption Fine Structure Study for Surface Events on a Pt_3Co/C Cathode Catalyst in a Polymer Electrolyte Fuel Cell during Voltage-Operating Processes

Nozomu Ishiguro,[†,‡] Takahiro Saida,[†] Tomoya Uruga,[§,⊥] Shin-ichi Nagamatsu,[⊥] Oki Sekizawa,[⊥] Kiyofumi Nitta,[§] Takashi Yamamoto,[⊥,∥] Shin-ichi Ohkoshi,[‡] Yasuhiro Iwasawa,[⊥] Toshihiko Yokoyama,[†,⊗] and Mizuki Tada*[,†,⊗]

[†]Institute for Molecular Science, 38 Nishigo-naka, Myodaiji, Okazaki, Aichi 444-8585, Japan

[‡]Department of Chemistry, Graduate School of Science, The University of Tokyo, 7-3-1 Hongo, Bunkyo-ku, Tokyo 113-0033, Japan

[§]Japan Synchrotron Radiation Research Institute, SPring-8, 1-1-1 Koto, Sayo, Hyogo 679-5198, Japan

[⊥]Innovation Research Center for Fuel Cells, The University of Electro-Communications, 1-5-1, Chofugaoka, Chofu, Tokyo 182-8585, Japan

[∥]Department of Mathematical and Material Sciences, Faculty of Integrated Arts and Sciences, The University of Tokushima, 1-1, Minamijosanjima-cho, Tokushima 770-8502, Japan

[⊗]The Graduate University for Advanced Studies (SOKENDAI), 38 Nishigo-naka, Myodaiji, Okazaki, Aichi 444-8585, Japan

Supporting Information

ABSTRACT: The structural kinetics of surface events on a Pt_3Co/C cathode catalyst in a polymer electrolyte fuel cell (PEFC) was investigated by operando time-resolved X-ray absorption fine structure (XAFS) with a time resolution of 500 ms. The rate constants of electrochemical reactions, the changes in charge density on Pt, and the changes in the local coordination structures of the Pt_3Co alloy catalyst in the PEFC were successfully evaluated during fuel-cell voltage-operating processes. Significant time lags were observed between the electrochemical reactions and the structural changes in the Pt_3Co alloy catalyst. The rate constants of all the surface events on the Pt_3Co/C catalyst were significantly higher than those on the Pt/C catalyst, suggesting the advantageous behaviors (cell performance and catalyst durability) on the Pt_3Co alloy cathode catalyst.

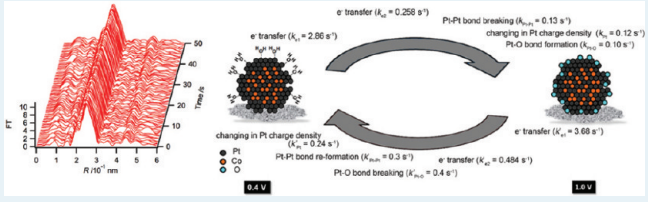

KEYWORDS: *fuel cell, PEFC, operando XAFS, time-resolved XAFS, Pt_3Co catalyst, structural kinetics*

INTRODUCTION

Polymer electrolyte fuel cells (PEFCs) are among the most efficient clean energy technologies, but practical application in automobiles remains challenging because of the high cost and insufficient durability of cathode catalysts under fuel-cell operating conditions.[1,2] A membrane electrode assembly (MEA) is utilized in a PEFC, which has a stacked structure consisting of an anode catalyst layer, a proton-conducting membrane electrolyte, and a cathode catalyst layer. Hydrogen is converted into protons and electrons on a metal catalyst at the anode catalyst surface, and the generated protons move to the cathode catalyst surface through the proton-conducting membrane, which contains highly acidic functional groups. At the cathode surface, protons and molecular oxygen react to produce water (oxygen reduction reaction; ORR) on a Pt-based catalyst. Unfavorable dissolution and deactivation of the Pt cathode catalyst under fuel-cell working conditions, however, is one of the most serious problems in PEFCs.[1−3]

Pt is considered to be the most durable metal catalyst, but the dissolution and subsequent sintering of expensive Pt catalysts nevertheless are a major hindrance to practical use. To improve fuel-cell performance and cathode catalyst durability, alloying of Pt with 3d transition metal elements such as Co, Ni, and Fe is a promising approach.[4−17] Pt-alloy surfaces can weaken binding of oxygenated species at cathodes[18] and intrinsic ORR activity is often enhanced by the addition of a second metal, resulting in better PEFC performance per Pt surface atom.[4−7,12−14,19−27]

Pt alloys have not only enhanced ORR activity but also significantly improved durability at the cathode.[4,15−17] Pt−Co alloy is a representative of the Pt-alloy cathode catalysts and has been reported to be more active and durable than Pt/C catalysts.[15] The origin of the superior fuel-cell performance of the Pt-alloy catalysts has been investigated by theoretical calculations,[27−33] scanning or transmission electron-microscopy (SEM or TEM),[4,14,34−36] electrochemical X-ray photoelectron

Received: April 5, 2012
Revised: May 10, 2012
Published: May 16, 2012

spectroscopy (EC-XPS),[37,38] and electrochemical impedance spectroscopy (EIS).[39] Several model structures have been proposed such as Pt-skin,[20] sandwich-segregation,[40] skeleton structures[13,20,34] for real Pt−Co particles in PEFCs. Acid treatment of Pt-3d metal alloy nanoparticles generally led to dissolution of the 3d metal to a skeleton structure that had a corrugated Pt-rich surface.[13,20,34] Thermal annealing[20] or potential-cycling[37] of the surface of skeleton structured nanoparticle reconstructs the surface to the so-called Pt-skin[20,37] or sandwich-segregation surface.[40] Although electrochemical surface events have been extensively investigated for both model systems such as single-crystal electrodes and practical PEFCs, the structural kinetics of the transformations of catalyst themselves and the ORR reaction mechanism on practical Pt−Co catalysts have not been established under the operating conditions of actual PEFC systems. Exploring these fundamental issues is expected to provide new insight into the development of advanced PEFC cathode catalysts.

X-ray absorption fine structure (XAFS) analysis has become a powerful tool for investigating the oxidation states and local coordination structures of supported metal catalysts under in situ reaction conditions.[6,11,41−49] A practical PEFC contains an abundance of water and fuel molecules, which prevents in situ measurements by methods such as Fourier transform infrared spectroscopy, transmission electron microscopy (TEM), and XPS. Time-resolved XAFS is a sophisticated technique that enables the study of the kinetics of dynamic reaction events involving metal catalysts.[46−61] We reported in situ time-resolved XAFS of a PEFC Pt/C cathode catalyst under operating conditions:[46] Quick-scan XAFS (QXAFS), which employs a new time-gating method with time resolution of 1 s, revealed the structural kinetics of a Pt/C cathode catalyst: eight rate constants of electron transfer, Pt charge density changes, and structural changes in the Pt nanoparticle catalyst were found to have significant time lags.[46]

In the present paper, we report the first study on the structural kinetics and surface reaction mechanism of a Pt_3Co/C cathode catalyst in an MEA during fuel-cell voltage-cycling processes. In situ time-resolved QXAFS spectra at the Pt L_{III}-edge and Co K-edge were measured at 500 ms intervals, and the analysis of the series of the operando QXAFS spectra for the PEFC bimetal cathode catalyst revealed the rate constants of electron transfer, changes in the charge density of Pt_3Co nanoparticles, and changes in the local coordination structures with Pt−Pt, Pt−Co, Co−Co, and Pt−O bonds. The operando analysis of the Pt_3Co/C and Pt/C catalysts elucidated the structural kinetics highly relevant to the advantageous performance of the Pt_3Co/C catalyst in a PEFC system.

EXPERIMENTAL SECTION

1. Fuel Cell. Pt/C (Tanaka Kikinzoku Kogyo Co. Ltd. (TKK), TEC10E50E; Pt 50 wt %) and Pt_3Co/C (TKK, TEC36E56E; 49 wt % metal (Pt and Co); 78 atom % Pt, 22 atom % Co) were used as cathode catalysts, and Pd/C (TKK, TECPdE50; Pd 50 wt %) was used as the anode catalyst (denoted as as-received powder). These catalysts were coated onto MEAs containing Nafion NR-212 (Sigma-Aldrich) membranes by Eiwa Co., Ltd. (denoted as as-prepared MEA). (Japan). The size of an MEA was 25 cm^2, and the catalyst loading at the cathode (Co or Pt) and anode (Pt) was 6 mg/cm^2.

A fabricated MEA was sandwiched in a laboratory-made single cell based on the Japan Automobile Research Institute (JARI) standard cell (Figure 1A and Supporting Information, Figure SI 1).[62] The in situ XAFS cell is composed of end plates

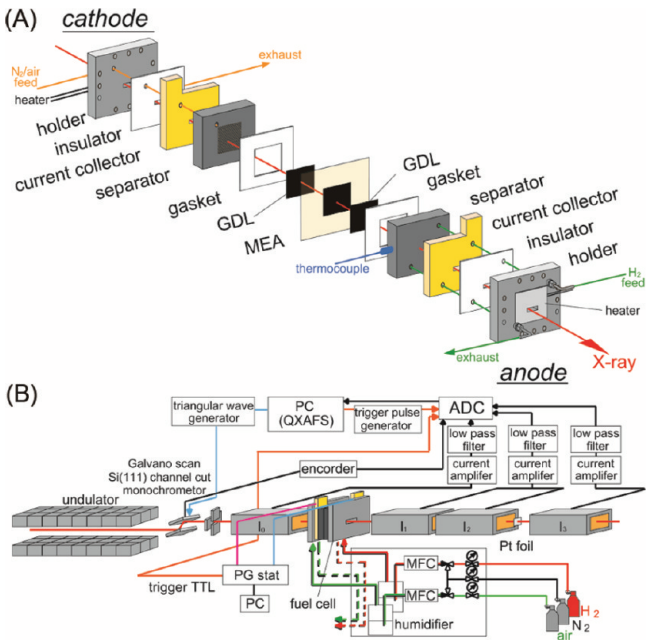

Figure 1. (A) Schematic of laboratory-made fuel cell for in situ XAFS measurements. (B) Setup of in situ time-resolved XAFS.

made of stainless steel (SUS316) and is equipped with a cartridge heater, epoxy resin insulators, Au-coated Cu current correctors, and carbon separators with grooved serpentine flow channels for gases. A similar stacking structure was used for both the anode and cathode, and the MEA was set between the anode and the cathode stacks (Figure 1A).

The flows of H_2 (G1 grade) to the anode and N_2 (G1 grade; XAFS measurements) or dry air (G1 grade; aging) to the cathode were regulated by mass-flow controllers and were bubbled through humidifiers at 351 K using a commercial gas supply kit (Eiwa Co., Ltd.). The humidified gases were supplied to the in situ XAFS cell heated at 353 K. Gas pressures and flow rates were 101.3 kPa and 300 mL min^{-1} at the anode (H_2), and 101.3 kPa and 900 mL min^{-1} at the cathode (N_2), respectively. A cell voltage between the anode and the cathode was controlled by a potentiostat/galvanostat (hereinafter, PG stat; Autolab; PGSTAT302N) with a current amplifier (Autolab; BOOSTER20A).

All MEAs were subjected to aging before in situ XAFS measurements. Dry air was fed to the cathode, and 14 constant current steps (0 → 0.06 → 0.09 → 0.33 → 0.45 → 0.63 → 0.78 → 0.96 → 1.41 → 1.95 → 3.90 → 5.82 → 9.72 → 11.67 A; 6 s per step) were repeated 150 times for aging. MEAs after the aging processes were not removed from cells after XAFS measurements. Cyclic voltammograms (CVs) were recorded with H_2 flow (anode) and N_2 flow (cathode) before and after XAFS measurements. The potential was swept between 0.05 and 0.9 V at 5 mV s^{-1}. The electrochemically accessible surface areas (ECSAs) of Pt_3Co/C and Pt/C cathode catalysts were calculated from the charge density of hydrogen adsorption on a Pt surface (210 $\mu C/cm_{-Pt}^2$).

2. Characterization. The X-ray diffraction (XRD) patterns of as-received Pt/C and Pt_3Co/C powders and of as-prepared and used MEAs were recorded on a Rigaku Multiflex-STe

dx.doi.org/10.1021/cs300228p | ACS Catal. 2012, 2, 1319−1330

diffractometer. The X-ray source, accelerating voltage, and tube current were Cu $K\alpha$ (λ = 0.15418 nm), 40 kV, and 40 mA, respectively. The XRD patterns were collected over a wide range (2θ = 15−95°) in continuous-scan mode, and over narrow range (2θ = 62−75°) in step-scan mode. The TEM images of Pt/C and Pt_3Co/C catalysts in as-prepared and used MEAs were acquired on a JEOL JEM-3200 apparatus (accelerating voltage: 300 kV). Scanning transmission electron microscopy/energy dispersive X-ray spectroscopy (STEM-EDS) analysis was performed on a JEOL JEM-ARM200F integrated with a JED-2300T system (accelerating voltage: 200 kV), and Pt $M\alpha$ and Co $K\alpha$ X-ray fluorescence was used to estimate the atomic percentage of Co in a Pt_3Co alloy particle.

3. In Situ QXAFS. In situ conventional QXAFS measurements were carried out at the BL01B1 beamline at SPring-8 (8.0 GeV, 100 mA). X-rays that emerged from a bending magnet were monochromatized by a Si(111) double-crystal monochromator. XAFS spectra were recorded in transmission mode. Incident (I_0) and transmitted (I_1) X-rays were detected by ion chambers filled with N_2 and N_2/Ar (75/25), respectively, for both Pt L_{III}-edge and Co K-edge XAFS measurements.

The voltage of a cell with an MEA after the aging treatment was controlled by the PG stat: 0.4 → 0.8 → 1.0 → 0.8 → 0.4 V. After 1 min at each voltage, Pt L_{III}-edge and Co K-edge QXAFS spectra were recorded (60 s/spectrum ×3 scans at the Pt L_{III}-edge and 60 s/spectrum ×4 scans at the Co K-edge) at each voltage. Each voltage step was held for 20 min (Supporting Information, Figure SI 2A).

4. In Situ Time-Resolved QXAFS. In situ time-resolved Pt L_{III}-edge QXAFS measurements were performed at the BL40XU beamline at SPring-8.[63] X-rays that emerged from a helical undulator were monochromatized by small Si(111) channel-cut monochromators equipped on a high-speed galvano scanner.[64] A series of QXAFS spectra was measured in transmission mode, and an in situ XAFS cell with an MEA after the aging treatment was set between I_0 and I_1/I_2 ion chambers. Pt foil was set between I_1/I_2 and I_3 ion chambers for the calibration of X-ray energies (Figure 1B). The ion chambers were filled with N_2 (I_0) or N_2/Ar (75/25) (I_1, I_2, and I_3).

A transistor-transistor logic signal (0 V → 5 V) was sent at t = 0 s from the PG stat connected to the XAFS cell to a PC that controlled the QXAFS measurements; the cell voltage was immediately switched from open-circuit voltage to 0.4 V by the PG stat. QXAFS measurements started at t = 84−87 s, and the cell voltage was increased from 0.4 to 1.0 V at t = 90 s. A series of QXAFS spectra was recorded every 500 ms (120 spectra over 60 s). At t = 174−177 s, the second continuous measurement of QXAFS spectra was carried out every 500 ms, and the cell voltage was decreased from 1.0 to 0.4 V at t = 180 s. At t = 270 s, the voltage was returned to open-circuit voltage (Supporting Information, Figure SI 2B).

5. Analysis of Pt L_{III}-Edge and Co K-Edge XAFS. The collected X-ray absorption near-edge structure (XANES) and Extended X-ray absorption fine structure (EXAFS) spectra were analyzed either in Ifeffit (Athena and Artemis),[65] or a custom program in Igor Pro 6.2. Background subtraction was performed using Autobk.[66] The white-line peak of a normalized Pt L_{III}-edge XANES spectrum was analyzed by curve fitting with an arctangent function and the following Lorentz function:

$$\mu t = \frac{a_1}{\pi}\left[\frac{\pi}{2} + \arctan\left(\frac{x - a_2}{a_3}\right)\right] + \frac{b_1}{1 + \left(\frac{x - b_2}{b_3}\right)^2} \quad (1)$$

Pt foil, $Pt(acac)_2$, and PtO_2 were used as standard materials to analyze the relationship between the white-line peak height of Pt L_{III}-edge XANES and Pt valence, and a linear relationship was observed for the compounds.

Extracted k^3-weighted Pt L_{III}-edge or Co K-edge EXAFS oscillations were Fourier transformed into R-space, in which curve-fitting analysis was carried out. The fitting parameters for each shell were coordination number (CN), interatomic distance (R), Debye−Waller factor (σ^2), and correction-of-edge energy (ΔE_0). Phase shifts and backscattering amplitude for each shell were calculated with FEFF8.4 code[57] using structural parameters obtained from the crystal structures of Pt, PtO_2, Pt_3Co, PtCo, Co, and CoO.[67−71] The amplitude reduction factors (S_0^2) of the Pt L_{III}-edge EXAFS of Pt foil and Co K-edge EXAFS of Co foil were estimated to be 0.94 and 0.72, respectively. R and ΔE_0 of a Pt−O shell, and σ^2 of all shells in Pt L_{III}-edge were fixed at their fitted values from Pt_3Co/C or Pt/C at 1.0 V (Supporting Information, Table SI 1). R of Co−Co and Co−Pt shells in Co K-edge were fixed at their fitted values from as-received Pt_3Co/C powder, and σ^2 of Co−Co and Co−Pt shells were fixed at their fitted values from Pt_3Co/C MEA at 0.4 V.

Error ranges of the curve-fitting analysis of the time-resolved QXANES spectra were estimated as 95% confidence intervals. Error ranges of the curve-fitting analysis of time-resolved EXAFS Fourier transforms were based on the definition in the Feffit code (Artemis). Seven parameters ((1) charge variation in a fuel cell recorded on the PG stat, (2) white-line height of Pt L_{III}-edge XANES, (3) CN of Pt−Pt, (4) CN of Pt−Co, (5) CN of Pt−O, (6) R of Pt−Pt, and (7) R of Pt−Co) were plotted against time t. The rate constants of these parameters were estimated by curve fitting using linear combinations of exponential curves. For the curve fitting, the initial and final values of each plot were calculated: the initial value of each parameter was the average of each parameter for the 5 s period before each voltage was applied; and its final value was the average of each parameter for the 5 s period before stopping each QXAFS measurement (Supporting Information, Figure SI 2B). Fitting with exponential curves was performed, taking into account error weighting at each point given by the inverse of error.

RESULTS

1. Cell Performance and Structure of Pt_3Co/C in MEA. A commercially available Pt_3Co/C alloy cathode catalyst (atomic ratio of Pt/Co = 3/1) was used to prepare an MEA, whose anode was composed of a Pd/C catalyst to avoid interference at the Pt L_{III}-edge. Cell performance using Pd/C as an anode catalyst was reported to be approximately 30% lower than that using Pt/C.[72] Although XAFS spectra for low Pt content catalysts were reported before,[73] we adopted higher cathode catalyst loading to improve S/N of time-resolved XAFS spectra in transmission mode for further analysis of structural kinetics.

Figures 2A and 2B show the CVs and power curves of the MEAs of the Pt_3Co/C and Pt/C cathode catalysts, and their ECSAs were estimated to be 5 × 10 m^2 g_{-Pt}^{-1} and 3 × 10 m^2 g_{-Pt}^{-1}, respectively. Pt oxidation in the positive-going scan and

dx.doi.org/10.1021/cs300228p | ACS Catal. 2012, 2, 1319−1330

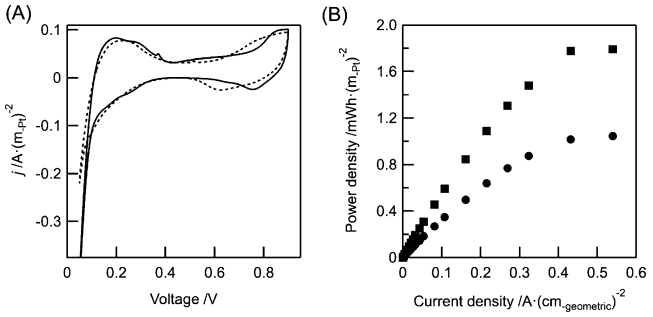

Figure 2. (A) Cyclic voltammograms of the Pt_3Co/C and Pt/C cathode catalysts in PEFCs recorded before in situ QXAFS measurements at SPring-8 BL01B1: solid line, Pt_3Co/C; and dotted line, Pt/C. (B) Power curves of the Pt_3Co/C and Pt/C cathode catalysts in the PEFCs: ■, Pt_3Co/C; and ●, Pt/C.

reduction in the negative-going scan between 0.6 and 0.9 V for the Pt_3Co/C MEA showed that the Pt_3Co catalyst was easier to reduce and more difficult to oxidize than the Pt/C catalyst. Similar behavior has been reported for Pt_3Co catalysts, suggesting that they have superior activity and durability in comparison with Pt particles.[4−6,24−26] The power density per unit ECSA of the Pt_3Co MEA was much larger than that of the Pt MEA (Figure 2B), also suggesting the good efficiency of the Pt_3Co alloy as a cathode catalyst.

The XRD patterns of Pt_3Co alloys are strongly dependent on the atomic ratio of Pt/Co.[14,69] As the atomic ratio of Co in a Pt face-centered cubic (fcc) structure becomes higher, the average bond distance (M−M; M = Pt or Co) in the alloy structure linearly decreases from 0.2772 nm (Pt, fcc)[67] to 0.2506 nm (Co, hexagonal close-packed (hcp)).[70] The theoretical XRD peak of the fcc (220) plane of Pt (67.6°) shifts to 69.1° (Pt_3Co), 70.5° (PtCo), and 75.9° (Co) (Supporting Information, Figure SI 3).[67,69,70]

The XRD peaks of the fcc (220) plane were observed at 67.3° and 69.4° for the as-received Pt/C and Pt_3Co/C powders, respectively, before MEA fabrication (Supporting Information, Figure SI 3). Accordingly, the average bond distances of M−M (M: Pt or Co) for the as-received Pt/C and Pt_3Co/C powders were estimated to be 0.278 and 0.270 nm, respectively. The observed average M−M distance of the Pt_3Co/C catalyst in an as-prepared MEA was 0.271 nm, which is similar to that of the as-received powder (0.270 nm) and that of Pt_3Co (0.272 nm).[69] The XRD analysis thus suggests that the original Pt_3Co alloy in the as-received sample was almost completely maintained in the as-prepared MEA. After XAFS measurements, the peak shift of the (220) plane was negligible (69.3° → 69.2°) as shown in Supporting Information, Figure SI 3 and Table SI 2, indicating that the alloy structure in the MEA also remained unchanged after the XAFS measurements.

The catalysts in the as-prepared MEA and used MEA after the XAFS measurements were examined by TEM (Supporting Information, Figure SI 4). The average size of Pt_3Co particles in the as-prepared MEA was estimated to be 5.3 ± 1.9 nm, and that in the used MEA was estimated to be 5.3 ± 2.0 nm. There was no significant change in the particle size distribution of the Pt_3Co catalyst in the MEA after the XAFS measurements. The (111) and (200) planes were primarily observed in both Pt_3Co/C MEAs, and the M−M bond distances estimated from the lattice images obtained by high-resolution TEM agreed with the average M−M distances estimated from the XRD patterns (Supporting Information, Table SI 2).

2. In Situ Pt L_{III}-Edge XAFS of Pt/C and Pt_3Co/C Catalysts. Figures 3A, 3B, and 3C show in situ Pt L_{III}-edge XANES, k^3-weighted EXAFS oscillations, and their Fourier transforms for the Pt_3Co/C and Pt/C MEAs at cell voltages of 0.4 and 1.0 V, measured by conventional QXAFS for 60 s at SPring-8 BL01B1. The oxidation of Pt was observed at 1.0 V in both the Pt_3Co/C and the Pt/C catalysts, but the increase in the Pt L_{III}-edge XANES white-line intensity of the Pt_3Co/C catalyst was smaller than that of the Pt/C catalyst (Figure 3A). The white-line heights, reflecting the 5d-electron density and valence state of Pt species, were estimated to be 0.42 at 0.4 V and 0.55 at 1.0 V (Pt/C), and 0.39 at 0.4 V and 0.45 at 1.0 V (Pt_3Co/C). The white-line height of Pt foil was estimated to be 0.44, which was similar to that of Pt/C catalyst at 0.4 V, but larger than that of the Pt_3Co/C catalyst at 0.4 V, indicating electron transfer from Co to Pt.

The structural parameters indicating the local coordination of the Pt_3Co/C and Pt/C catalysts were also examined by curve-fitting analysis of the Pt L_{III}-edge EXAFS Fourier transforms (Figure 3C and Supporting Information, Table SI 1). There were contributions of Pt−O at 0.201 nm and Pt−Pt at 0.275 ±

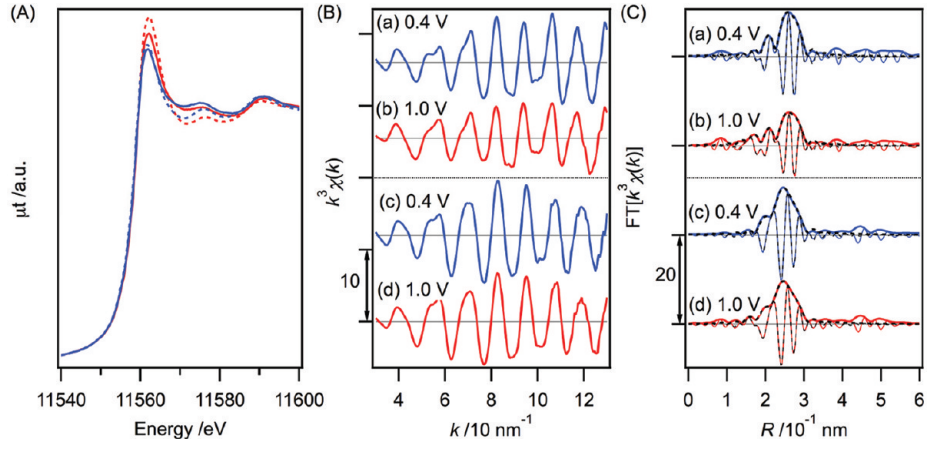

Figure 3. In situ Pt-L_{III} edge XAFS spectra at 0.4 and 1.0 V for the Pt/C and Pt_3Co/C MEAs (60 s × 3 scan). (A) Pt L_{III}-edge XANES spectra: blue dashed line, Pt/C at 0.4 V; red dashed line, Pt/C at 1.0 V; blue solid line, Pt_3Co/C at 0.4 V; and red solid line, Pt_3Co/C at 1.0 V. (B) k^3-Weighted Pt L_{III}-edge EXAFS oscillations and (C) their Fourier transforms (Pt/C: k = 30−140 nm^{-1}, Pt_3Co/C: k = 30−130 nm^{-1}): solid line, experimental data; and dashed line, fitted data. (a) Pt/C at 0.4 V, (b) Pt/C at 1.0 V, (c) Pt_3Co/C at 0.4 V, and (d) Pt_3Co/C at 1.0 V.

dx.doi.org/10.1021/cs300228p | ACS Catal. 2012, 2, 1319−1330

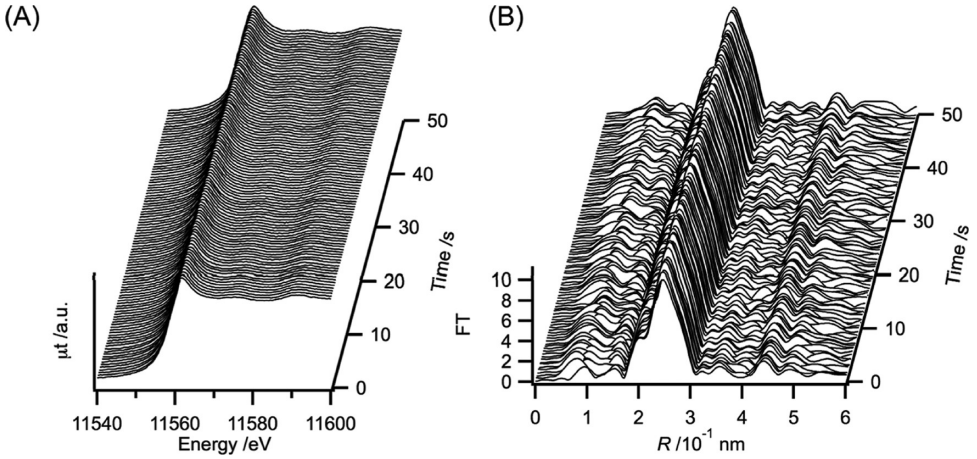

Figure 4. Series of in situ time-resolved Pt L_{III}-edge XAFS spectra for Pt_3Co/C MEA. XAFS spectra were recorded at 500 ms intervals at SPring-8 BL40XU. (A) Series of in situ time-resolved Pt L_{III}-edge XANES spectra for the voltage-cycling process of 0.4 V → 1.0 V. (B) Series of in situ time-resolved k^3-weighted Pt L_{III}-edge EXAFS Fourier transforms at k = 30−130 nm^{-1} for the voltage-cycling process of 1.0 V → 0.4 V.

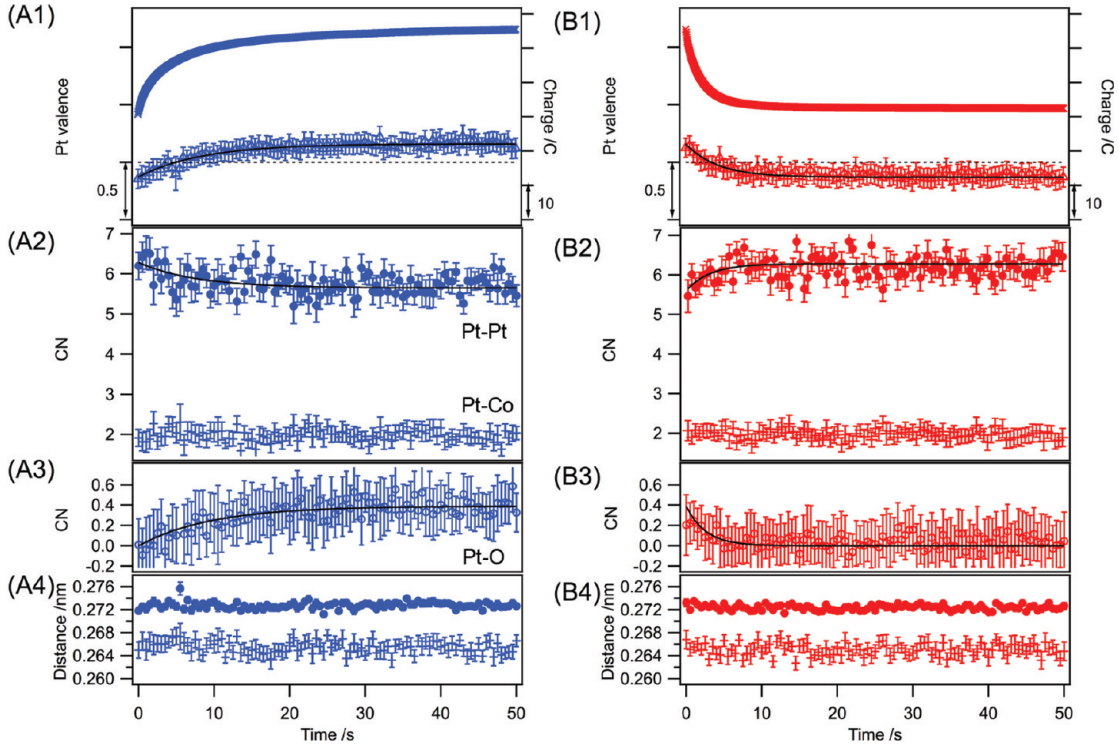

Figure 5. Time profiles of (1) electric charge and Pt valence on an equivalent scale, (2) CNs of Pt−Pt and Pt−Co bonds, (3) CN of Pt−O bonds, and (4) R of Pt−Pt and Pt−Co bonds for the voltage-cycling processes on Pt_3Co/C. (A) 0.4 V → 1.0 V and (B) 1.0 V → 0.4 V. k = 30−130 nm^{-1}; R = 0.10− 0.31 nm. ×: electrical charge in the cell, Δ: Pt valence, ●:Pt−Pt, +:Pt−Co, and ○:Pt−O. Dashed lines in (A1) and (B1) correspond to be the valence state of Pt foil. The intervals on the right and left axes in (1) were scaled to be identical (in coulombs).

0.001 nm for the Pt/C catalyst, where the EXAFS Fourier transforms for the Pt_3Co/C catalyst were successfully fitted with three shells (Pt−O, Pt−Co, and Pt−Pt). At 0.4 V, the CNs of Pt−Co and Pt−Pt were 1.8 ± 0.2 at 0.266 ± 0.001 nm and 6.3 ± 0.3 at 0.272 ± 0.001 nm, respectively, and no positive contribution of Pt−O was observed. At 1.0 V, the CNs of Pt−O, Pt−Co, and Pt−Pt were 0.6 ± 0.1 at 0.205 nm, 1.8 ± 0.1 at 0.266 ± 0.001 nm, and 5.5 ± 0.1 at 0.273 ± 0.001 nm, respectively, indicating that the surface of Pt−Co alloy was oxidized at 1.0 V.

3. In Situ Time-Resolved QXAFS at Pt L_{III}-Edge of the Pt_3Co/C MEA. A series of in situ time-resolved QXAFS spectra was successfully recorded every 500 ms during voltage-cycling processes (0.4 V → 1.0 V → 0.4 V) (Figure 4 and Supporting Information, Figure SI 5). We found similar changes in the white-line heights of the Pt L_{III}-edge QXANES spectra as shown in Supporting Information, Figure SI 6A. The white-line heights of these QXANES spectra were estimated by curve fitting and plotted against time t (Figure 5 (1)).

Fine EXAFS oscillations at the Pt L_{III}-edge were recorded in the k range of 30−130 nm^{-1} by QEXAFS measurements with acquisition time of 500 ms (Supporting Information, Figure SI 6B). Their Fourier transforms were fitted with three shells (Pt−O, Pt−Co, and Pt−Pt) as shown in Supporting Information,

dx.doi.org/10.1021/cs300228p | ACS Catal. 2012, 2, 1319−1330

Figure SI 6C and Table SI 3. R and ΔE_0 of Pt−O and σ^2 of all shells were fixed at corresponding values determined by curve fitting to the conventional EXAFS spectra obtained with an acquisition time of 60 s (Supporting Information, Table SI 2). We detected changes in the CNs of Pt−Pt and Pt−O by time-resolved XAFS during fuel-cell operation at different voltages (Supporting Information, Table SI 3).

The operando time-resolved QXAFS measurements of the Pt_3Co/C cathode catalyst revealed eight kinetics parameters (Figure 5): (1) charge in the fuel cell recorded on the PG stat, showing electron transfer in the fuel cell; (2) charge density of Pt estimated from the white-line height of the Pt L_{III}-edge XANES; (3) CN of Pt−Pt; (4) CN of Pt−Co; (5) CN of Pt−O; (6) R of Pt−Pt; (7) R of Pt−Co; and (8) R of Pt−O. These parameters were estimated for both voltage operations (0.4 V → 1.0 and 1.0 V → 0.4 V). Charge (1), Pt valence (2), CN of Pt−Pt (3), and CN of Pt−O (5) showed significant differences during the voltage-cycling processes, while CN of Pt−Co (4), R of Pt−Pt (6), and R of Pt−Co (7) were almost constant as shown in Figure 5.

The changes in these four parameters (1, 2, 3, and 5) were fitted with exponential curves to determine their rate constants (Table 1 and Supporting Information, Table SI 4). The rate constants in the 0.4 V → 1.0 V process are indicated with k, and those in the 1.0 V → 0.4 V process are indicated with k'. The changes in charge (1) in the fuel cell were fitted with two exponential curves. The rate constants of fast electron transfer (k_{e1} and k'_{e1}) were 2.86 ± 0.04 s^{-1} and 3.68 ± 0.03 s^{-1}, respectively; the rate constants of slow electron transfer (k_{e2} and k'_{e2}) were 0.258 ± 0.003 s^{-1} and 0.484 ± 0.002 s^{-1}, respectively. The details of these two electron transfer types are not clear at the moment, but they may be related to electric double layer current and the changes in the charge density of the Pt_3Co alloys, and the charge profile could not be fitted with one exponential curve.

Table 1. Rate Constants of Kinetics Parameters for the Pt_3Co/C and Pt/C MEAs in Voltage-Cycling Processes Estimated by Operando Time-Resolved XAFS at Pt L_{III}-Edge

		rate constant (k, k') /s^{-1}	
process	parameter	Pt_3Co/C	Pt/C
0.4 V → 1.0 V (k)	(2) XANES white-line height	0.12 ± 0.02	0.073 ± 0.001
	(3) CN (Pt−Pt)	0.13 ± 0.03	0.088 ± 0.008
	(4) CN (Pt−Co)	no change	
	(5) CN (Pt−O)	0.10 ± 0.03	0.076 ± 0.009
	(1) charge in the fuel cell[a]	2.86 ± 0.04 0.258 ± 0.003	1.84 ± 0.02 0.167 ± 0.001
1.0 V → 0.4 V (k')	(2) XANES white-line height	0.24 ± 0.05	0.14 ± 0.03
	(3) CN (Pt−Pt)	0.3 ± 0.1	0.078 ± 0.009
	(4) CN (Pt−Co)	no change	
	(5) CN (Pt−O)	0.4 ± 0.2	0.11 ± 0.02
	(1) charge in the fuel cell[a]	3.68 ± 0.03 0.484 ± 0.002	2.16 ± 0.01 0.259 ± 0.001

[a]The rate constants of the charge in the fuel cell were estimated by curve fitting of changes in currents in the fuel cell recorded on the PG stat.

The changes in charge density of Pt (2), which is determined from the white-line height of Pt L_{III}-edge XANES, were fitted with an exponential curve. Their rate constants (k_{Pt} and k'_{Pt}) were estimated to be 0.12 ± 0.02 s^{-1} and 0.24 ± 0.05 s^{-1}. There is a linear relationship between the charge density of Pt valence electrons and the white-line height of the Pt L_{III}-edge, and thus the intensity was converted to the change of Pt valence electrons (in coulombs). The changes in charge amplitude of the cathode (in coulombs) and of Pt valence electrons (in coulombs) were different from each other as shown in Figure 5A1, and the latter was much smaller than the former.[46]

The variations in the CNs of Pt−Pt (3) and Pt−O (5) were fitted with an exponential curve, whose rate constants (k_{Pt-Pt}, k'_{Pt-Pt}, k_{Pt-O}, and k'_{Pt-O}) were estimated to be 0.13 ± 0.03 s^{-1}, 0.3 ± 0.1 s^{-1}, 0.10 ± 0.03 s^{-1}, and 0.4 ± 0.2 s^{-1}, respectively (Table 1 and Supporting Information, Table SI 4). The ΔCN values for Pt−Pt and Pt−O were 0.63 and 0.39, respectively (Figure 5 (2) and (3) and Supporting Information, Table SI 4). The ΔCN value for Pt−O indicated that the surface of Pt_3Co alloy was covered by oxygenated species at 1.0 V. The CN of Pt−Pt returned to its original value at 0.4 V following the 1.0 V → 0.4 V process, indicating that the dissolution of Pt was negligible for operation at voltages of 0.4−1.0 V.

Note that there were no significant changes in CN of Pt−Co (4) (Figure 5 (2)). The constant CN of Pt−Co suggests that the oxidation of Co species on the Pt_3Co/C catalyst was negligible in the investigated voltage range. These results agreed with structural information from the Co K-edge XAFS described later. These rate constants were ordered as follows: k_{e1} (2.86 s^{-1}) ≫ k_{e2} (0.258 s^{-1}) > k_{Pt-Pt} (0.13 s^{-1}) ≈ k_{Pt} (0.12 s^{-1}) ≈ k_{Pt-O} (0.10 s^{-1}) (0.4 V → 1.0 V), and k'_{e1} (3.68 s^{-1}) ≫ k'_{e2} (0.484 s^{-1}) ≈ k'_{Pt-O} (0.4 s^{-1}) ≈ k'_{Pt-Pt} (0.3 s^{-1}) ≈ k'_{Pt} (0.24 s^{-1}) (1.0 V → 0.4 V) (Table 1). The changes in R of Pt−Pt (6) and Pt−Co (7) were barely observed (Figure 5 (4)).

4. In Situ Co *K*-Edge XAFS of Pt_3Co/C Catalyst. In situ Co K-edge EXAFS spectra of the Pt_3Co/C catalyst were also measured by conventional QXAFS at SPring-8 BL01B1. Figure 6 shows Co K-edge XANES spectra, k^3-weighted EXAFS

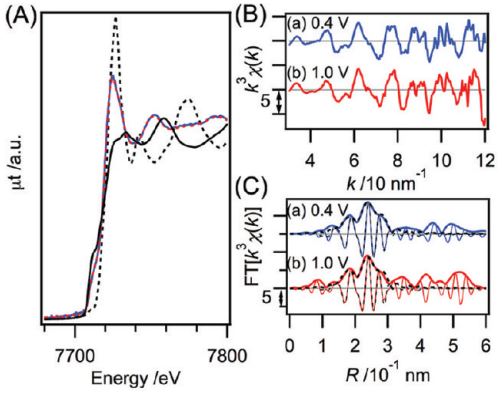

Figure 6. In situ Co K-edge XAFS at 0.4 and 1.0 V for the Pt_3Co/C catalyst (60 s × 4 scan). (A) Co K-edge XANES spectra: black solid line, Co foil; black dashed line, CoO; blue solid line, Pt_3Co/C at 0.4 V; and red dashed line, Pt_3Co/C at 1.0 V. (B) Co K-edge k^3-weighted EXAFS oscillations and (C) their Fourier transforms at k = 30−120 nm^{-1}: solid line, experimental data; dashed line, fitted data; (a) Pt_3Co/C at 0.4 V and (b) Pt_3Co/C at 1.0 V.

dx.doi.org/10.1021/cs300228p | ACS Catal. 2012, 2, 1319−1330

Table 2. Structural Parameters Estimated by the Curve-Fitting Analysis of in Situ Co *K*-Edge EXAFS Fourier Transforms at 0.4 and 1.0 V for the Pt_3Co/C Catalysts and Related Co Compounds[a]

sample (*R* factor%)	shell	CN	*R* /nm	ΔE_0 /eV	σ^2 /10^{-5} nm^2
(a) Co foil (R_f = 0.03%)[b]	Co−Co	12.0 ± 0.3	0.250 ± 0.001	10.3 ± 0.3	6.4 ± 0.2
(b) CoO (R_f = 1.3%)[c]	Co−O	6.5 ± 1.5	0.213 ± 0.002	15 ± 3	7.8 ± 0.2
	Co−Co	12.5 ± 0.7	0.301 ± 0.001	11 ± 2	6.7
(c) as-received Pt_3Co/C powder at 10 K (R_f = 0.04%)[d]	Co−Co	3.4 ± 1.1	0.262 ± 0.003	8 ± 3	8.7 ± 0.3
	Co−Pt	5.9 ± 1.5	0.268 ± 0.001	9 ± 2	2.6 ± 0.1
(d) Pt_3Co/C MEA at 0.4 V (R_f = 1.9%)[e]	Co−O	1.8 ± 0.9	0.203 ± 0.004	4 ± 7	5 ± 5
	Co−Co	4.6 ± 1.5	0.262	6 ± 3	20.3
	Co−Pt	5.4 ± 0.6	0.268	10 ± 1	5.8
(e) Pt_3Co/C MEA at 1.0 V (R_f = 2.7%)[e]	Co−O	1.3 ± 0.7	0.203 ± 0.003	9 ± 8	1 ± 4
	Co−Co	4.9 ± 1.8	0.262	7 ± 4	20.3
	Co−Pt	5.1 ± 0.7	0.268	10 ± 2	5.8

[a]See Figure 6) (k = 30−120 nm^{-1}. [b]R = 0.13−0.27 nm. [c]R = 0.10−0.31 nm. σ^2 of Co−Co was fixed at the value when CN of Co−Co was 12.0. [d]R = 0.16−0.31 nm. [e]R = 0.10−0.31 nm. *R*s of Co−Co and Co−Pt were fixed at the values of (c). σ^2s of Co−Co and Co−Pt were fixed at the fitted results of Pt−Co/C at 0.4 V.

oscillations, and their Fourier transforms for the Pt_3Co/C catalyst at 0.4 and 1.0 V. In contrast to the Pt L_{III}-edge XANES, the change in the white-line intensity at the Co *K*-edge was negligible at the investigated cell voltages (Figure 6A).

The Co *K*-edge EXAFS Fourier transforms were fitted with three shells (Co−O, Co−Co, and Co−Pt) as shown in Table 2. The Co−Pt and Co−Co distances (*R*) were estimated by curve-fitting analysis of Co *K*-edge EXAFS Fourier transform of the as-received Pt_3Co/C powder before MEA fabrication, and were 0.268 ± 0.001 nm and 0.262 ± 0.003 nm, respectively. This Co−Pt bond distance (0.268 nm) was consistent with the Pt−Co bond distance (0.266 nm) determined from the Pt L_{III}-edge EXAFS Fourier transforms. The Co−Co distance (0.262 nm) was longer than that of pure Co (0.251 nm), suggesting that the Co−Co bond was ascribed to that in Pt−Co alloys not to discrete Co particles.

Because of the limited number of Co atoms in the MEA, the Co−Co and Co−Pt bond distances were fixed for the EXAFS curve-fitting analysis of the MEA. The CNs for Co−O, Co−Co, and Co−Pt in an MEA at 0.4 V were estimated to be 1.8 ± 0.9, 4.6 ± 1.5, and 5.4 ± 0.6 (Table 2). In contrast to the structural parameters around Pt determined from the Pt L_{III}-edge EXAFS, the CNs and *R* of the Co−O, Co−Co, and Co−Pt bonds were almost similar at 0.4 and 1.0 V. These results indicate that discrete oxidized Co species with the Co−O bonds were present in the MEA, and they did not respond to the voltage-cycling operation,[43] resulting in the negligible changes in the Co *K*-edge XANES and EXAFS. In situ time-resolved XANES at Co *K*-edge provided similar results.

5. STEM Analysis of Pt_3Co/C Catalyst. Figure 7 shows the STEM image and line profile of a Pt_3Co particle taken out from an MEA after the in situ XAFS measurements. The line profile of a Pt_3Co particle of 4.37 nm in diameter showed that the distribution of Co atoms in the nanoparticle was not uniform. Co was scarce at the surface, but became more abundant at the particle core (Figure 7B). The Co percentages were about 15−20% at the core and less than 10% at the surface.

The commercial as-received Pt_3Co/C powders from TKK were subjected to acid leaching to remove Co from the surface of Pt_1Co_1 nanoparticles; this procedure gives a skeleton Pt_3Co alloy structure.[4,14,34,35,74] When an MEA made with the skeleton-type Pt_3Co particles was subjected to the aging process, it was reported that Pt atoms on the surface were reconstructed to form a Pt-skin structure with PtCo alloy core

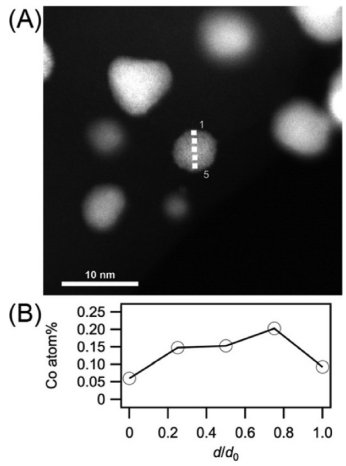

Figure 7. (A) STEM image of Pt_3Co/C extracted from the MEA after in situ time-resolved XAFS measurements. (B) The line profile of Co atom % for a Pt_3Co alloy particle in (A) (dotted line) by EDS analysis. d_0 = 4.37 nm.

and Pt-rich skin, which is Pt-rich reconstructed surface.[4,37] STEM analysis revealed a similar tendency for the used Pt_3Co/C catalyst.[4,14,36] These results agreed with the results of the in situ Pt L_{III}-edge and Co *K*-edge XAFS analyses.

6. In Situ Time-Resolved QXAFS at Pt L_{III}-Edge of Pt/C Catalyst. In situ time-resolved QXAFS of the Pt/C catalyst was measured similarly to the Pt_3Co/C catalyst during the voltage-cycling processes (0.4 V → 1.0 V → 0.4 V) (Supporting Information, Figure SI 7). Time-resolved QXAFS spectra at the Pt L_{III}-edge were acquired every 500 ms, and the EXAFS Fourier transforms were fitted with two shells (Pt−O and Pt−Pt) (Supporting Information, Figure SI 8 and Table SI 5). The charges in the fuel cell, the white-line intensity of the Pt L_{III}-edge XANES, the CNs of Pt−O and Pt−Pt bonds, and the bond distance of Pt−Pt were plotted against time *t* as shown in Supporting Information, Figure SI 9.

R of Pt−Pt was found to be constant during the voltage-cycling process (Supporting Information, Figure SI 9 (4)), but other four parameters were fitted with exponential curves to estimate the rate constants for the changes of these parameters (Supporting Information, Table SI 6). Charges in the fuel cell were fitted with the linear combination of two exponential curves. In the fuel cell, the rate constants for fast electron

dx.doi.org/10.1021/cs300228p | ACS Catal. 2012, 2, 1319−1330

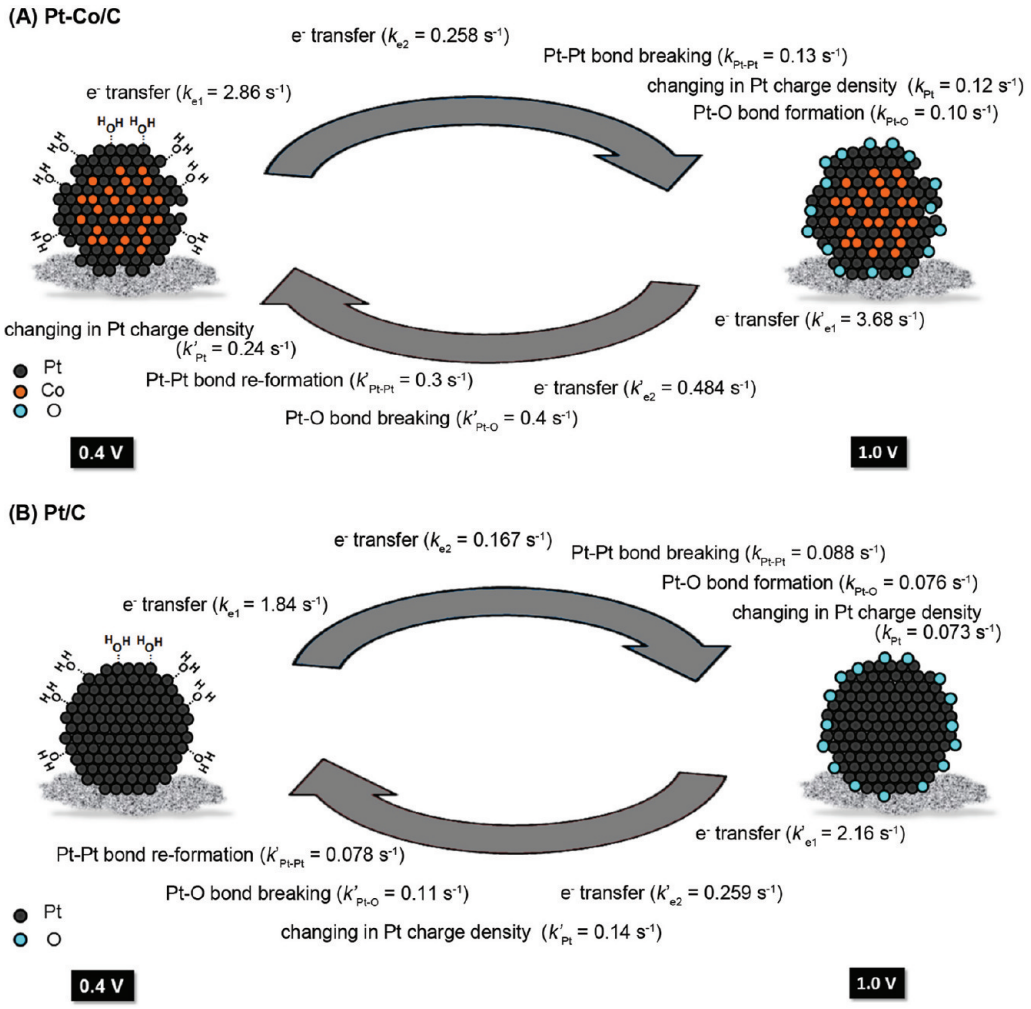

Figure 8. Proposed structural kinetics of the surface events on the (a) Pt_3Co/C and (b) Pt/C cathode catalysts for the voltage cycling processes at 353 K. Each voltage-cycling process can be regarded to be reversible.

transfer (k_{e1} and k'_{e1}) were 1.84 ± 0.02 s^{-1} and 2.16 ± 0.01 s^{-1}, respectively, and those for slow electron transfer (k_{e2} and k'_{e2}) were 0.167 ± 0.001 s^{-1} and 0.259 ± 0.001 s^{-1}, respectively. They could not be fitted with only one exponential curve.

In contrast, the changes in charge density in Pt during the voltage-cycling process (0.4 V → 1.0 V) could be fitted with one exponential curve. Their rate constants (k_{Pt} and k'_{Pt}) were estimated to be 0.073 ± 0.001 s^{-1}/0.14 ± 0.03 s^{-1}. The charge amplitudes in the fuel cell (in coulombs) and the Pt charge density (in coulombs) were different from each other (Supporting Information, Figure SI 9 (1)), and the latter was much smaller than the former. These results are similar to those of the Pt_3Co/C catalyst.

The changes in CN for Pt−Pt and Pt−O were fitted with an exponential curve, whose rate constants k_{Pt-Pt}, k'_{Pt-Pt}, k_{Pt-O}, and k'_{Pt-O} were found to be 0.088 ± 0.008 s^{-1}, 0.078 ± 0.009 s^{-1}, 0.076 ± 0.009, and 0.11 ± 0.02 s^{-1}, respectively (Supporting Information, Table SI 6). ΔCN of Pt−Pt and Pt−O were 0.72 and 0.42, respectively. Accompanied by the decrease in the ΔCN of Pt−Pt (= 0.72), oxygen penetrated into the subsurface of the Pt particles at 1.0 V. The decrease in Pt−Pt CN to its initial value at 0.4 V, indicating that the dissolution of Pt was negligible at voltages of 0.4−1.0 V.

The rate constants were ordered as follows: k_{e1} (1.84 s^{-1}) ≫ k_{e2} (0.167 s^{-1}) > k_{Pt-Pt} (0.088 s^{-1}) ≈ k_{Pt-O} (0.076 s^{-1}) ≈ k_{Pt} (0.073 s^{-1}) (0.4 → 1.0 V), and k'_{e1} (2.16 s^{-1}) ≫ k'_{e2} (0.259 s^{-1}) > k'_{Pt} (0.14 s^{-1}) ≈ k'_{Pt-O} (0.11 s^{-1}) ≈ k'_{Pt-Pt} (0.078 s^{-1}) (1.0 V → 0.4 V). Changes in the Pt−Pt bond distance were barely observed (Supporting Information, Figure SI 9 (4)).

DISCUSSION

1. Structures of Pt_3Co/C Alloy Catalysts. Pt and Co can be alloyed at any Pt/Co compositions, and their packing structures and metal−metal bond distances depend on the Pt/Co composition.[69,75] Co has an hcp structure, and Pt has an fcc structure and Pt_xCo_{1-x} ($x \geq 0.25$) alloys usually have fcc structures. There is a linear relationship between the average interatomic distance of M−M (M: Pt or Co) and the Co composition x.[69] The M−M distances of pure Pt and pure Co are 0.2772 nm[67] and 0.2506 nm,[70] respectively, and average M−M distances (average of Pt−Pt, Pt−Co, and Co−Co bond distances) in Pt_xCo_{1-x} ($0 < x < 1$) are in the middle of them. Although the average M−M distances depend on the disordering of Pt and Co atoms in the alloys, the average M−M distances of Pt_3Co and PtCo alloys are generally 0.272 and 0.267 nm in fcc units, respectively (Supporting Information, Table SI 2).[69]

The commercial Pt_3Co/C precursor with Pt/Co atomic ratio = 3/1 (as-received powder) is prepared by acid etching of Pt_1Co_1 alloy nanoparticles; the material prepared in this way is

dx.doi.org/10.1021/cs300228p | ACS Catal. 2012, 2, 1319−1330

reported to be Pt_3Co alloy nanoparticles with a skeleton-type structure.[4] Indeed, the average M−M bond distance of the as-received Pt_3Co/C powder was estimated to be 0.270 nm by XRD, which was almost consistent with the Co composition in Pt_3Co alloy (0.272 nm). On an MEA, the average M−M bond distance (0.271 nm) was observed to be similar to that of the powder. It has been reported that the aging procedure, which entails repeated applications of increased current at decreased cell potential in galvanostatic operation mode, causes reconstruction of the surface of the skeleton-type Pt−Co alloy particles and produces a Pt−Co alloy core with a Pt-rich skin.[4,37] A STEM line profile of a used MEA suggested the formation of such a Pt-rich skin alloy particle, though the line profile did not have atomic scale position resolution (Figure 7).

At 0.4 V, the Pt−Co alloy nanoparticles at the cathode seem to be reduced to metallic states. The CN and average bond distance of Pt−Pt in an MEA at 0.4 V was estimated to be 6.3 at 0.272 nm (Pt−Pt from Pt L_{III}-edge), which was shorter than that of pure Pt (0.277 nm)[67] and as long as that of Pt_3Co alloy from XRD pattern (0.272 nm);[69] those of Pt−Co were estimated to be 1.8 at 0.266 nm (Pt−Co from Pt L_{III}-edge) and 5.4 at 0.268 nm (Co−Pt from Co *K*-edge), whose bond distances (0.266−0.268 nm) were similar to that of Pt_1Co_1 alloy from XRD (0.267 nm);[69] that of Co−Co was estimated to be 4.6 at 0.262 nm (Co−Co from Co *K*-edge), which was longer than that of pure Co (0.251 nm)[70] (Table 2, Supporting Information, Tables SI 1 and SI 2). These bond distances elucidated that these bonds were attributed to those in the Pt−Co alloy particles and not in discrete Pt or Co particles and agreed with the Pt-skin Pt−Co alloy structure proposed before.[14,36,48,75] The Pt−Co/Co−Pt bond distance implied that the composition of the Pt−Co alloy core was similar to PtCo alloy, and the average observed bond distance of Pt−Pt (0.272 nm >0.267 nm (Pt−Co)) seemed to be obtained from both the PtCo alloy core and the Pt-rich skin.

The longer Co−Co distance in the MEA (0.262 nm) compared to that of pure Co (0.251 nm) indicated that discrete metallic Co particles were negligible in the MEA and these Co−Co bonds were attributed to those in the Pt−Co alloy core. The negligible change at the Co *K*-edge with cell voltage (Figure 6) implies that Co atoms at the core of the Pt−Co alloy particle with the Pt-rich skin do not directly contribute the ORR reaction on the surfaces of the Pt−Co alloy catalysts in the voltage-cycling processes. These results are consistent with the proposed Pt−Co alloy model with the Co-poor, Pt-rich skin,[14,36,48,75] as illustrated in Figure 8.

2. Structural Kinetics of the Surface Events on the Pt_3Co/C Cathode Catalyst for the Voltage-Cycling Processes. Electrochemical analysis provides kinetics data about electrochemical reactions; however, the structural kinetics of metal catalysts for promoting electrochemical reactions cannot be obtained by the conventional electrochemical analysis. XAFS is a useful technique for determining the local coordination structures of metal catalysts under operating conditions, which are often highly related to catalytic performance. In situ time-resolved XAFS has been used to study active heterogeneous catalysts under reaction conditions.[46−61] The ability of hard X-rays to penetrate solid materials enables acquisition of the XAFS spectra of practical metal catalysts in fuel cells under real operating conditions where fuel and water are present.

At 0.4 V, the CN of Pt−O bonds were negligible on the Pt_3Co/C catalyst, and it was 0.39 at 1.0 V (Supporting Information, Table SI 4). The observed CN of Pt−O suggests that the surface of the Pt_3Co nanoparticle (average diameter = 5.3 nm) was fully covered by oxygenated species at 1.0 V. The decrease of 0.63 in CN (Supporting Information, Table SI 4) in the Pt−Pt bond at 1.0 V was observed; the formation of the oxygenated species breaks the Pt−Pt bonds at the surface of the Pt-rich skin on the Pt−Co nanoparticles.

Oxygen species on the Pt catalyst surfaces at the cathode have been investigated by DFT calculations,[31−33,76] EC-XPS,[38,66] EIS,[39,77] and XAFS,[47−49] and several oxygen species were reported including Pt−OH_{ads}, surface Pt−O_{ads}, and Pt−O. The formation of surface Pt−O_{ads} and Pt−O would be accompanied with the stretching or dissociation of Pt−Pt bonds, and these oxygen species have been reported on Pt(111) and polycrystalline surfaces.[32,48,49] The shorter distance of Pt−O at 0.205 nm than that of Pt−OH at 0.22 nm previously reported,[48] and the decrease in the CN of Pt−Pt bonds at 1.0 V observed by in situ XAFS analysis implied the formation of surface Pt−O_{ads} and Pt−O on the Pt-rich skin of the Pt_3Co alloy particles at 1.0 V.

We succeeded in determining the rate constants for the surface events at the PEFC Pt_3Co/C cathode catalyst by operando time-resolved XAFS recorded every 500 ms. The rate constants of the cathode surface events on the Pt_3Co/C cathode catalyst in the voltage-cycling processes were in the following order (Figure 8):

0.4 V → 1.0 V:

$$k_{e1}(2.86\ s^{-1}) >> k_{e2}(0.258\ s^{-1}) > k_{Pt-Pt}(0.13\ s^{-1}) \approx k_{Pt}(0.12\ s^{-1}) \approx k_{Pt-O}(0.10\ s^{-1})$$

1.0 V → 0.4 V:

$$k'_{e1}(3.68\ s^{-1}) >> k'_{e2}(0.484\ s^{-1}) \approx k'_{Pt-O}(0.4\ s^{-1}) \approx k'_{Pt-Pt}(0.3\ s^{-1}) \approx k'_{Pt}(0.24\ s^{-1})$$

A significant difference was observed between fast electron transfer and structural changes in the Pt_3Co catalyst for the voltage-cycling processes. The first electron transfer (k_{e1} and k'_{e1}) was probably caused by the formation of electric double layers, and they were much faster than the rate constants of subsequent reactions. In the voltage-cycling process (0.4 V → 1.0 V), the second electron transfer was probably related to the catalyst surface events, and then Pt−Pt bond breaking, changing in Pt charge density, and Pt−O bond formation proceeded with similar reaction rates (Figure 8). The differences between the rate constants of the latter three processes were extremely small and the formation of the Pt−O bonds may initiate the surface reactions accompanied by the breaking of Pt−Pt bonds to give Pt at a higher oxidation state.

The reverse process (1.0 V → 0.4 V) also began with fast electron transfer, and then the second electron transfer and Pt−O bond breaking proceeded at similar rates. Pt−Pt bond reformation and discharging reduction in Pt oxidation state had similar rate constants to Pt−O bond breaking (Figure 8). Note that there are time lags in the structural kinetics at the PEFC Pt_3Co/C cathode catalyst surface.

The constant value of the CN of Pt−Co bonds during the voltage-cycling processes strongly suggests that Co atoms negligibly contribute to catalyzing oxidation reactions at the PEFC cathode. In the electrochemical reaction on the Pt_3Co alloy catalyst in a half-cell in 0.5 M H_2SO_4, similar behavior has also been reported.[48] Co species located at the core of the Pt−

Co alloy particles could not react with oxygen and the oxidation reaction proceeded on Pt at the Pt-rich skin surface of the Pt_3Co alloy particles, resulting in negligible changes in the Co *K*-edge XANES and EXAFS spectra (Figure 6).

3. Effects of Adding Co to Pt in Structural Kinetics and PEFC Performance. It has been proposed that the alloying of Co to Pt weakens binding of oxygenated species on the alloy particles and enhances intrinsic ORR activity.[4−6,12−14,20−26] DFT calculations and XPS studies have indicated that the energy level of the Pt *d*-band center is lowered by the addition of Co to Pt.[19,21,27−29,36] The red-shift of the Pt *d*-band center agrees with the decrease in the intensity of Pt L_{III}-edge white-line intensity on the Pt_3Co catalyst (Figure 3 (A)).

We compared the reaction mechanism and structural kinetics on the Pt_3Co/C and Pt/C catalysts under similar fuel-cell operating conditions. The orders of the rate constants for the Pt/C catalyst without Co were as follows (Figure 8),

0.4 V → 1.0 V:

$$k_{e1}(1.84\ s^{-1}) > > k_{e2}(0.167\ s^{-1}) > k_{Pt-Pt}(0.088\ s^{-1}) \approx k_{Pt-O}(0.076\ s^{-1}) \approx k_{Pt}(0.073\ s^{-1})$$

1.0 V → 0.4 V:

$$k'_{e1}(2.16\ s^{-1}) > > k'_{e2}(0.259\ s^{-1}) > k'_{Pt}(0.14\ s^{-1}) \approx k'_{Pt-O}(0.11\ s^{-1}) \approx k'_{Pt-Pt}(0.078\ s^{-1})$$

The time lags in these rate constants for electron transfer and structural changes were also observed for the Pt/C catalyst, similarly to our previous study where different reaction conditions were used.[46] Electron transfer proceeded rapidly and then the rate of structural changes of the Pt catalyst gradually increased to the electron transfer rate. The order of easiness for the voltage-operating process may be different from that for the Pt_3Co/C catalyst, but the difference in the three events was small and thus could not be evaluated. However, the reaction mechanism of these surface events appears similar to that on the Pt-rich surface of a Pt−Co alloy nanoparticle.

It is to be noted that all the rate constants on the Pt_3Co/C catalyst were larger than the corresponding rate constants on the Pt/C catalysts (Figure 8). During the 1.0 V → 0.4 V process, for example, Pt−Pt bond breaking on the Pt_3Co/C catalyst was 1.5-fold to that on the Pt/C catalyst. The rate constant of Pt−O bond breaking (k'_{Pt-O}), which is highly related to the ORR activity of the cathode catalyst, was about 4 times higher on Pt−Co/C (0.4 s^{-1}) than on Pt/C (0.11 s^{-1}). There was also a significant difference in the rate constant of Pt−Pt bond reformation (k'_{Pt-Pt}), on Pt_3Co/C (0.3 s^{-1}) and Pt/C (0.078 s^{-1}), which may be relevant for realizing better catalyst durability of the Pt_3Co/C catalyst.

These higher reaction rates are thought to be closely related to fuel-cell performance of the Pt_3Co/C catalyst. In general, Pt nanoparticle cathode catalysts in PEFCs are irreversibly oxidized and gradually dissolve as a result of voltage cycling under fuel-cell operating conditions.[78] These phenomena occur to a greater extent in air. The oxidative dissolution of the Pt species and growth of Pt particles ultimately cause the irreversible deactivation of the cathode catalyst, which is among the most serious problems in PEFCs. For Pt_3Co alloy catalysts, theoretical and experimental studies have found that surface O species on Pt_3Co particles interfere with the further oxidation of the alloy particles compared to Pt catalysts.[32,48]

The irreversible oxidation of the Pt catalysts depends on the difference in rate between oxidation and reduction of the Pt catalysts during voltage cycling.[3,79] The oxidation of Pt proceeds at 1.0 V, whereas the reverse reduction may proceed slow and only partially on Pt catalysts without Co when cell voltage is controlled to 0.4 V. The repeated cycling on oxidized Pt species which could not be recovered causes extensive dissolution of the Pt cathode catalyst.[4,15,35] Although the CV in Figure 2A suggests that the Pt_3Co catalyst was more easily reduced and less easily oxidized than the Pt catalyst without Co, Pt_3Co alloy systems facilitate reversible oxidation/reduction in the voltage-cycling processes.[13,21,25,26] The structural kinetics determined from the in situ time-resolved XAFS in Figure 8 revealed that all the rate constants of the surface events on the Pt_3Co/C cathode catalyst were higher than those on Pt/C, particularly the reduction steps involving Pt−O bond breaking. Reversible redox cycles on Pt_3Co alloys are suggested as a key factor in the superior performance of Pt_3Co alloy cathode catalysts in PEFCs. Understanding of the fundamental issues of the structural kinetics of the catalyst surface events by in situ time-resolved XAFS establishes new boundaries for the regulation and operation of fuel cells.

CONCLUSIONS

We acquired a series of in situ time-resolved QXAFS spectra for PEFC Pt_3Co/C and Pt/C cathode catalysts in a JARI single cell at 500 ms intervals. The systematic analysis of the time-resolved QXAFS spectra provided 10 rate constants of the dynamic surface events on the Pt_3Co/C catalyst in voltage-cycling processes between 0.4 and 1.0 V. Redox reactions proceeded on the surface of the Pt−Co alloy nanoparticles having a Pt-rich skin, and a similar reaction mechanism was found for the Pt_3Co/C catalyst and the Pt/C catalyst. However, large increases in these rate constants, particularly those for the reduction processes of Pt−O bond breaking, Pt−Pt bond reformation, and change in the charge density of Pt were observed through addition of Co to Pt. The structural kinetics of the catalyst transformations are suggested to be closely related to the fuel-cell performance and high catalyst durability of Pt_3Co alloy catalyst.

ASSOCIATED CONTENT

Supporting Information

The detail of in situ XAFS measurements, EXAFS curve-fitting results, XRD, TEM, fitting results for kinetics parameters, and ref 1. This material is available free of charge via the Internet at http://pubs.acs.org.

AUTHOR INFORMATION

Corresponding Author

*E-mail: mtada@ims.ac.jp.

Funding

This work was supported by the New Energy and Industrial Technology Development Organization of the Ministry of Economy, Trade and Industry in Japan. XAFS measurements were performed under SPring-8 No. 2010B1014 (BL01B1), 2010B1017 (BL40XU), 2011A1031 (BL01B1), and 2011A1033 (BL40XU).

Notes

The authors declare no competing financial interest.

■ ACKNOWLEDGMENTS

We thank JEOL for STEM-EDS measurements.

■ REFERENCES

(1) Borup, R.; et al. *Chem. Rev.* **2007**, *107*, 3904.
(2) Schmittinger, W.; Vahidi, A. *J. Power Sources* **2008**, *180*, 1.
(3) De Bruijn, F. A.; Dam, V. A. T.; Janssen, G. J. M. *Fuel Cells* **2008**, *8*, 3.
(4) Chen, S.; Gasteiger, H. A.; Hayakawa, K.; Tada, T.; Shao-Horn, Y. *J. Electrochem. Soc.* **2010**, *157*, A82.
(5) Mukerjee, S.; Srinivasan, S. *J. Electroanal. Chem.* **1993**, *357*, 201.
(6) Mukerjee, S.; Srinivasan, S.; Soriaga, M. P.; McBreen, J. *J. Electrochem. Soc.* **1995**, *142*, 1409.
(7) Mani, P.; Srivastava, R.; Stasser, P. *J. Phys. Chem. C* **2008**, *112*, 2770.
(8) Santiago, E. I.; Varanda, L. C.; Villullas, H. M. *J. Phys. Chem. C* **2007**, *111*, 3146.
(9) Markovic, N. M.; Schmidt, T. J.; Stamenkovic, V.; Ross, P. N. *Fuel Cells* **2001**, *1*, 105.
(10) Paulus, U. A.; Wokaun, A.; Scherer, G. G.; Schmidt, T. J.; Stamenkovic, V.; Radmilovic, V.; Markovic, N. M.; Ross, P. N. *J. Phys. Chem. B* **2002**, *106*, 4181.
(11) Zhang, J.; Lima, F. H. B.; Shao, M. H.; Sasaki, K.; Wang, J. X.; Hanson, J.; Adzic, R. R. *J. Phys. Chem. B* **2005**, *109*, 22701.
(12) Koh, S.; Toney, M. F.; Strasser, P. *Electrochim. Acta* **2007**, *52*, 2765.
(13) Stamenkovic, V. R.; Mun, B. S.; Arenz, M.; Mayrhofer, K. J. J.; Lucas, C. A.; Wang, G.; Ross, P. N.; Markovic, N. M. *Nat. Mater.* **2007**, *6*, 241.
(14) Chen, S.; Sheng, W.; Yabuchi, N.; Ferreira, P. J.; Allard, L. F.; Shao-Horn, Y. *J. Phys. Chem. C* **2009**, *113*, 1109.
(15) Yu, P.; Pemberton, M.; Plasse, P. *J. Power Sources* **2005**, *144*, 11.
(16) Colón-Mercado, H. R.; Popov, B. N. *J. Power Sources* **2006**, *155*, 253.
(17) Matsutani, K.; Hayakawa, K.; Tada, T. *Platinum Met. Rev.* **2010**, *54*, 223.
(18) Menning, C. A.; Hwu, H. H.; Chen, J. G. *J. Phys. Chem. B* **2006**, *110*, 15471.
(19) Stamenkovic, V. R.; Fowler, B.; Mun, B. S.; Wang, G.; Ross, P. N.; Lucas, C. A.; Marcović, N. M. *Science* **2007**, *315*, 493.
(20) Stamenkovic, V. R.; Mun, B. S.; Mayhofer, K. J. J.; Ross, P. N.; Markovic, N. M. *J. Am. Chem. Soc.* **2006**, *128*, 8813.
(21) Hwang, B. J.; Kumar, S. M.; Chen, C.-H.; Monalisa; Cheng, M.-Y.; Liu, D.-G.; Lee, J.-F. *J. Phys. Chem. C* **2007**, *111*, 15267.
(22) Lee, M. H.; Do, J. S. *J. Power Sources* **2009**, *188*, 353.
(23) Loukrakpam, R.; Luo, J.; He, T.; Chen, Y. S.; Xu, Z.; Njoki, P. N.; Wanjala, B. N.; Fang, B.; Mott, D.; Yin, J.; Klar, J.; Powell, B.; Zhong, C.-J. *J. Phys. Chem. C* **2011**, *115*, 1682.
(24) Oezaslan, M.; Strasser, P. *J. Power Sources* **2011**, *196*, 5240.
(25) Mani, P.; Srivastava, R.; Strasser, P. *J. Power Sources* **2011**, *196*, 666.
(26) Koh, S.; Leisch, J.; Toney, M. F.; Strasser, P. *J. Phys. Chem. C* **2007**, *111*, 3744.
(27) Kitchin, J. R.; Nørskov, J. K.; Barteau, M. A.; Chen, J. G. *J. Chem. Phys.* **2004**, *120*, 10240.
(28) Stamenkovic, V.; Mun, B. S.; Mayrhofer, K. J. J.; Ross, P. N.; Markovic, N. M.; Rossmeisl, J.; Greeley, J.; Nørskov, J. K. *Angew. Chem., Int. Ed.* **2006**, *45*, 2897.
(29) Mun, B. S.; Watanabe, M.; Rossi, M.; Stamenkovic, V.; Markovic, N. M.; Ross, P. N. *J. Chem. Phys.* **2005**, *123*, 204717.
(30) Nørskov, J. K.; Rossmeisl, J.; Logadottir, A.; Lindqvist, L.; Kitchin, J. R.; Bligaard, T.; Jónsson, H. *J. Phys. Chem. B* **2004**, *108*, 17886.
(31) Xu, Y.; Ruban, A. V.; Mavrikakis, M. *J. Am. Chem. Soc.* **2004**, *126*, 4717.
(32) Hirunsit, P.; Balbuena, P. B. *Surf. Sci.* **2009**, *603*, 3239.
(33) Callejas-Tovar, R.; Balbuena, P. B. *Surf. Sci.* **2008**, *602*, 3531.
(34) Carlton, C. E.; Chen, S.; Ferreira, P. J.; Allard, L. F.; Shao-Horn, Y. *J. Phys. Chem. Lett.* **2012**, *3*, 161.
(35) Xin, H. L.; Mundy, J. A.; Liu, Z.; Cabezas, R.; Hoven, R.; Kourkoutis, L. F.; Zhang, J.; Subramanian, N. P.; Makharia, R.; Wagner, F. T.; Muller, D. A. *Nano Lett.* **2011**, *12*, 490.
(36) Lai, F.-J.; Su, W.-N.; Sarma, L. S.; Liu, D.-G.; Hsieh, C.-A.; Lee, J.-F.; Hwang, B.-J. *Chem.—Eur. J.* **2010**, *16*, 4602.
(37) Doung, H. T.; Rigsby, M. A.; Zhou, W.-P.; Wieckowski, A. *J. Phys. Chem. C* **2007**, *111*, 13460.
(38) Wakisaka, M.; Suzuki, H.; Mitsui, S.; Uchida, H.; Watanabe, M. *J. Phys. Chem. C* **2008**, *112*, 2750.
(39) Wakabayashi, N.; Takeuchi, M.; Uchida, H.; Watanabe, M. *J. Chem. Phys. B* **2005**, *109*, 5836.
(40) Gauthier, Y. *Surf. Rev. Lett.* **1996**, *3*, 1663.
(41) Russell, A. E.; Rose, A. *Chem. Rev.* **2004**, *104*, 4613.
(42) Antolini, E.; Salgado, J. R. C.; Giz, M. J.; Gonzalez, E. R. *Int. J. Hydrogen Energy* **2005**, *30*, 1213.
(43) Witkowska, A.; Dsoke, S.; Principi, E.; Marassi, R.; Di Cicco, A.; Albertini, V. R. *J. Power Sources* **2008**, *178*, 603.
(44) Lewis, E. A.; Kendrick, I.; Jia, Q.; Grice, C.; Sergre, C. U.; Smotkin, E. S. *Electrochim. Acta* **2011**, *56*, 8827.
(45) Melke, J.; Schoekel, A.; Gerteisen, D.; Dixon, D.; Ettinshausen, F.; Cremers, C.; Roth, C.; Ramaker, D. E. *J. Phys. Chem. C* **2012**, *116*, 2838.
(46) Tada, M.; Murata, S.; Asaoka, T.; Hiroshima, K.; Okumura, K.; Tanida, H.; Uruga, T.; Nakanishi, H.; Matsumoto, S.; Inada, Y.; Nomura, M.; Iwasawa, Y. *Angew. Chem., Int. Ed.* **2007**, *46*, 4310.
(47) Friebel, D.; Miller, D. J.; O' Grady, C. P.; Anniyev, T.; Bargar, J.; Bergmann, U.; Ogasawara, H.; Wikfeldt, K. T.; Pettersson, L. G. M.; Nilsson, A. *Phys. Chem. Chem. Phys.* **2011**, *13*, 262.
(48) Imai, H.; Matsumoto, M.; Miyazaki, T.; Kato, K.; Tanida, H.; Uruga, T. *Chem. Commun.* **2011**, *47*, 3538.
(49) Imai, H.; Izumi, K.; Matsumoto, M.; Kubo, Y.; Kato, K.; Imai, Y. *J. Am. Chem. Soc.* **2009**, *131*, 6293.
(50) Uemura, Y.; Inada, Y.; Bando, K. K.; Sasaki, T.; Kamiuchi, N.; Eguchi, K.; Yagishita, A.; Nomura, M.; Tada, M.; Iwasawa, Y. *J. Phys. Chem. C* **2011**, *115*, 5823.
(51) Uemura, Y.; Inada, Y.; Bando, K. K.; Sasaki, T.; Kamiuchi, N.; Eguchi, K.; Yagishita, A.; Nomura, M.; Tada, M.; Iwasawa, Y. *Phys. Chem. Chem. Phys.* **2011**, *13*, 15833.
(52) Tada, M.; Uemura, Y.; Bal, R.; Inada, Y.; Nomura, M.; Iwasawa, Y. *Phys. Chem. Chem. Phys.* **2010**, *12*, 5701.
(53) Newton, M. A.; Jyoti, B.; Dent, A. J.; Fiddy, S. G.; Evans, J. *Chem. Commun.* **2004**, *21*, 2382.
(54) Alayon, E. M. C.; Singh, J.; Nachtegaal, M.; Harfouche, M.; van Bokhoven, J. A. *J. Catal.* **2009**, *263*, 228.
(55) Nikitenko, S.; Beale, A. M.; van der Eerden, A. M. J.; Jacques, S. D. M.; Leynaud, O.; O'Brien, M. G.; Detollenaere, D.; Kaptein, R.; Weckhuysen, B. M.; Bras, W. *J. Synchrotron Radiat.* **2008**, *15*, 632.
(56) Lamberti, C.; Pretipino, C.; Bonino, F.; Capello, L.; Bordiga, S.; Spoto, G.; Zecchina, A.; Moreno, S. D.; Cremaschi, B.; Garilli, M.; Marsella, A.; Carmello, D.; Vidotto, S.; Leofanti, G. *Angew. Chem., Int. Ed.* **2002**, *41*, 2341.
(57) Muddada, N. B.; Olsbye, U.; Caccialupi, L.; Cavani, F.; Leofanti, G.; Gianolio, D.; Bordiga, S.; Lamberti, C. *Phys. Chem. Chem. Phys.* **2010**, *12*, 5605.
(58) Newton, M. A.; Belver-Colderia, C.; Martínez-Arias, A.; Fernández-García, M. *Nat. Mater.* **2007**, *6*, 528.
(59) Newton, M. A.; van Beek, W. *Chem. Soc. Rev.* **2010**, *39*, 4845.
(60) Newton, M. A. *Chem. Soc. Rev.* **2008**, *37*, 2644.
(61) Nagai, Y.; Dohmae, K.; Ikeda, Y.; Takagi, N.; Tanabe, T.; Hara, N.; Guilera, G.; Pascarelli, S.; Newton, M. A.; Kuno, O.; Jiang, H.; Shinjoh, H.; Matsumoto, S. *Angew. Chem., Int. Ed.* **2008**, *47*, 9303.
(62) Hashimasa, Y.; Numata, T.; Moriya, K.; Watanabe, S. *JARI Res. J.* **2002**, *24*, 455.
(63) Hara, T.; Tanaka, T.; Seike, T.; Bizen, T.; Maréchal, X.; Kohda, T.; Inoue, K.; Oka, T.; Suzuki, T.; Yagi, N.; Kitamura, H. *Nucl. Instrum. Methods Phys. Res., Sect. A* **2001**, *467–468*, 165.

(64) Uruga, T.; Tanida, H.; Inoue, K.; Yamazaki, H.; Irie, T. In *Proceedings of the 13th International Conference on X-Ray Absorption Fine Structure*, Stanford, CA, July 9−14, 2006; American Institute of Physics: College Park, MD, 2006.
(65) Newville, M.; Ravel, B.; Haskel, D.; Rehr, J. J.; Stern, E. A.; Yacoby, Y. *Phys. B* **1995**, *208−209*, 154.
(66) Ravel, B.; Newville, M. *J. Synchrotron Radiat.* **2005**, *12:4*, 537.
(67) Davey, W. P. *Phys. Rev.* **1925**, *25*, 753.
(68) Muller, O.; Roy, R. *J. Less-Common Met.* **1968**, *16*, 129.
(69) Buschow, K. H. J.; van Engen, P. G.; Jongebreur, R. *J. Magn. Magn. Mater.* **1983**, *38*, 1.
(70) Mueller, S.; Scholten, P. *Z. Angew. Phys.* **1966**, *20*, 498.
(71) Tombs, N. C.; Rooksby, H. P. *Nature* **1950**, *165*, 442.
(72) Takeguchi, T.; Anzai, Y.; Kikuchi, R.; Eguchi, K.; Ueda, W. *J. Electrochem. Soc.* **2007**, *154*, B1132.
(73) Principi, E.; Witowska, A.; Dsoke, S.; Marassi, R.; Di Cicco, A. *Phys. Chem. Chem. Phys.* **2009**, *11*, 9987.
(74) Watanabe, M.; Tsurumi, K.; Mizukami, T.; Nakamura, T.; P. Stonehart, P. *J .Electrochem. Soc.* **1994**, *141*, 2659.
(75) Greco, G.; Witowska, A.; Principi, E.; Minicucci, M.; Di Cicco, A. *Phys. Rev. B* **2011**, *83*, 134103.
(76) Ogasawara, H.; Brena, B.; Nordlund, D.; Nyberg, M.; Pelmenschikov, A.; Pettersson, L. G. M.; Nilsson, A. *Phys. Rev. Lett.* **2002**, *89*, 276102.
(77) Wakisaka, M.; Suzuki, H.; Mitsui, S.; Uchida, H.; Watanabe, M. *Langmuir* **2009**, *25*, 1897.
(78) Bondarenko, A. S.; Stephens, I. E. L.; Hansen, H. A.; Pérez-Alonso, F. J.; Tripkovic, V.; Johansson, T. P.; Rossmeisl, J.; Nørskov, J. K.; Chorkendorff, I. *Langmuir* **2011**, *27*, 2058.
(79) Burke, L. D.; Burkley, D. T. *J. Electroanal. Chem.* **1994**, *366*, 239.